AFRL-AFOSR-VA-TR-2016-0136

Premixed Turbulent Combustion in High Reynolds Number Regimes of Thickened Flamelets and Distributed Reactions

James Driscoll
UNIVERSITY OF MICHIGAN

03/24/2016
Final Report

Air Force Research Laboratory
AF Office Of Scientific Research (AFOSR)/ RTA1
Arlington, Virginia 22203
Air Force Materiel Command

REPORT DOCUMENTATION PAGE

Form Approved
OMB No. 0704-0188

PLEASE DO NOT RETURN YOUR FORM TO THE ABOVE ORGANIZATION.

1. REPORT DATE *(DD-MM-YYYY)*	2. REPORT TYPE	3. DATES COVERED *(From - To)*
11-02-2016	Final	15-03-2012 to 14-03-2015

4. TITLE AND SUBTITLE
Premixed Turbulent Combustion in High Reynolds Number Regimes of Thickened Flamelets and Distributed Reactions

5a. CONTRACT NUMBER
FA9550-12-1- 0101

5b. GRANT NUMBER
11024186

5c. PROGRAM ELEMENT NUMBER

6. AUTHOR(S)
James F. Driscoll

5d. PROJECT NUMBER

5e. TASK NUMBER

5f. WORK UNIT NUMBER

7. PERFORMING ORGANIZATION NAME(S) AND ADDRESS(ES)
University of Michigan, Department of Aerospace
Engineering, 1320 Beal Ave. Ann Arbor MI 48109-2140

8. PERFORMING ORGANIZATION REPORT NUMBER

9. SPONSORING/MONITORING AGENCY NAME(S) AND ADDRESS(ES)
AFOSR, Dr. Chiping Li, 875 North Randolph Street, Suite 325. Arlington, VA 22203

10. SPONSOR/MONITOR'S ACRONYM(S)

11. SPONSOR/MONITOR'S REPORT NUMBER(S)

12. DISTRIBUTION/AVAILABILITY STATEMENT
Unclassified Unlimited

13. SUPPLEMENTARY NOTES

14. ABSTRACT
The physics of turbulent premixed flames, in the range of the high Reynolds numbers that are associated with Air Force applications, was measured for the first time using advanced laser imaging diagnostics. Combustion in three regimes on the Borghi regime diagram of premixed turbulent flames was quantified for the first time, by imaging the thicknesses of preheat and reaction layers. New PLIF diagnostics were developed, due to our interactions with Dr. Cam Carter at AFRL to image reactions zones with a new CH PLIF method, as well as using the overlap method that involves formaldehyde and OH PLIF. Results are used to assess previous theoretical predictions of regime boundaries. PLIF images of CH, OH and formaldehyde were obtained for thirteen cases. The three regimes are (a) the thickened preheat (TP) regime that is bounded by the Klimov-Williams limit, (b) the broken reaction layers (BR) boundary and the partially-distributed reactions (PDR) regime. A new Hi-Plot burner provides "extremely-turbulent" flames which is ten times the turbulence level of previous experiments.

15. SUBJECT TERMS
propulsion, combustion, turbulence, augmentor

16. SECURITY CLASSIFICATION OF:			17. LIMITATION OF ABSTRACT	18. NUMBER OF PAGES	19a. NAME OF RESPONSIBLE PERSON
a. REPORT	b. ABSTRACT	c. THIS PAGE			James F. Driscoll
U	U	U	UU	24	19b. TELEPHONE NUMBER *(Include area code)* 734 936-0101

Reset

INSTRUCTIONS FOR COMPLETING SF 298

1. REPORT DATE. Full publication date, including day, month, if available. Must cite at least the year and be Year 2000 compliant, e.g. 30-06-1998; xx-06-1998; xx-xx-1998.

2. REPORT TYPE. State the type of report, such as final, technical, interim, memorandum, master's thesis, progress, quarterly, research, special, group study, etc.

3. DATES COVERED. Indicate the time during which the work was performed and the report was written, e.g., Jun 1997 - Jun 1998; 1-10 Jun 1996; May - Nov 1998; Nov 1998.

4. TITLE. Enter title and subtitle with volume number and part number, if applicable. On classified documents, enter the title classification in parentheses.

5a. CONTRACT NUMBER. Enter all contract numbers as they appear in the report, e.g. F33615-86-C-5169.

5b. GRANT NUMBER. Enter all grant numbers as they appear in the report, e.g. AFOSR-82-1234.

5c. PROGRAM ELEMENT NUMBER. Enter all program element numbers as they appear in the report, e.g. 61101A.

5d. PROJECT NUMBER. Enter all project numbers as they appear in the report, e.g. 1F665702D1257; ILIR.

5e. TASK NUMBER. Enter all task numbers as they appear in the report, e.g. 05; RF0330201; T4112.

5f. WORK UNIT NUMBER. Enter all work unit numbers as they appear in the report, e.g. 001; AFAPL30480105.

6. AUTHOR(S). Enter name(s) of person(s) responsible for writing the report, performing the research, or credited with the content of the report. The form of entry is the last name, first name, middle initial, and additional qualifiers separated by commas, e.g. Smith, Richard, J, Jr.

7. PERFORMING ORGANIZATION NAME(S) AND ADDRESS(ES). Self-explanatory.

8. PERFORMING ORGANIZATION REPORT NUMBER. Enter all unique alphanumeric report numbers assigned by the performing organization, e.g. BRL-1234; AFWL-TR-85-4017-Vol-21-PT-2.

9. SPONSORING/MONITORING AGENCY NAME(S) AND ADDRESS(ES). Enter the name and address of the organization(s) financially responsible for and monitoring the work.

10. SPONSOR/MONITOR'S ACRONYM(S). Enter, if available, e.g. BRL, ARDEC, NADC.

11. SPONSOR/MONITOR'S REPORT NUMBER(S). Enter report number as assigned by the sponsoring/ monitoring agency, if available, e.g. BRL-TR-829; -215.

12. DISTRIBUTION/AVAILABILITY STATEMENT. Use agency-mandated availability statements to indicate the public availability or distribution limitations of the report. If additional limitations/ restrictions or special markings are indicated, follow agency authorization procedures, e.g. RD/FRD, PROPIN, ITAR, etc. Include copyright information.

13. SUPPLEMENTARY NOTES. Enter information not included elsewhere such as: prepared in cooperation with; translation of; report supersedes; old edition number, etc.

14. ABSTRACT. A brief (approximately 200 words) factual summary of the most significant information.

15. SUBJECT TERMS. Key words or phrases identifying major concepts in the report.

16. SECURITY CLASSIFICATION. Enter security classification in accordance with security classification regulations, e.g. U, C, S, etc. If this form contains classified information, stamp classification level on the top and bottom of this page.

17. LIMITATION OF ABSTRACT. This block must be completed to assign a distribution limitation to the abstract. Enter UU (Unclassified Unlimited) or SAR (Same as Report). An entry in this block is necessary if the abstract is to be limited.

Final PERFORMANCE REPORT

Principal Investigator:	James F. Driscoll
Institution:	University of Michigan, Department of Aerospace Engineering, 1320 Beal Ave. Ann Arbor MI 48109-2140 Dr. Chiping Li
Project Monitor	
Project Title:	Premixed Turbulent Combustion in High Reynolds Number Regimes of Thickened Flamelets and Distributed Reactions
Project Number:	FA9550-12-1- 0101
Project Period:	March 15, 2012 to March 14, 2015 + no cost extension February 11, 2016
Report Date:	

Summary of Results:

The physics of turbulent premixed flames, in the range of the high Reynolds numbers that are associated with Air Force applications, was measured for the first time using advanced laser imaging diagnostics. Combustion in three regimes on the Borghi regime diagram of premixed turbulent flames was quantified for the first time, by imaging the thicknesses of preheat and reaction layers. New PLIF diagnostics were developed, due to our interactions with Dr. Cam Carter at AFRL to image reactions zones with a new CH PLIF method, as well as using the overlap method that involves formaldehyde and OH PLIF. Results are used to assess previous theoretical predictions of regime boundaries. PLIF images of CH, OH and formaldehyde were obtained for thirteen cases. The three regimes are (a) the thickened preheat (TP) regime that is bounded by the Klimov-Williams limit, (b) the broken reaction layers (BR) boundary that is bounded by Norbert Peters predicted limit, and the partially-distributed reactions (PDR) regime. A new Hi-Plot burner provides "extremely-turbulent" flames (defined to be values of u'/S_L between 24 and 243) which is up to ten times that of previous experiments.

It was found that the measured thickened preheat (TP) boundary is in approximate agreement with the Klimov-Williams prediction, but that the broken flamelet (BF) boundary measurements do not agree with the Peters prediction. Partially distributed reactions (PDR) are local blobs of distributed reactions that are connected by thin flamelets. They were found to be associated with either merging or breaking of the flamelets. Globally-distributed reactions were not observed. There was no evidence that distributed reaction occur due solely to layer broadening, as has been predicted. Preheat layer thickness was ten times the laminar value but reaction layers were not broadened. Residence time of eddies in the flame (which scales as x/U) is important since the flame tip has reactions that are broader, broken and more distributed than at the flame base.

Nomenclature

BR = broken reaction layer boundary
DR = distributed reaction zone boundary
Ka = Karlovitz number of Peters (Eq. 1) equal to $(\delta_{F,L} / \eta_K)^2$
Ka_δ = Karlovitz number of Peters (Eq. 5) based on reaction zone thickness $(\delta_{RZ,L} / \eta_K)^2$
Re_T = turbulent Reynolds number $(u' \lambda_I / \nu)$
S_L = laminar flame speed
TP = thickened preheat layer boundary
u' = r.m.s. velocity fluctuation in reactants
U = mean velocity of reactants
Greek symbols:
λ_I = integral scale in reactants

$\delta_{F,L}$ = laminar flame thickness (Eq. 2), = $(T_2-T_1)/(dT/dx)_{max}$
$\delta_{PH,L}$ = laminar preheat layer thickness
$\delta_{RZ,L}$ = laminar reaction layer thickness
η_K = Kolmogorov length scale

Introduction

There are several reasons why research has been needed to measure the new physics that occur in the high Reynolds number premixed turbulent flame regimes that are associated with Air Force applications. The regimes of interest include those of thin and thickened flamelets as well as broken and distributed reactions. One reason is to understand when certain modeling assumptions are valid and when they fail. Models that can predict flameout and heat transfer within engines are important to Air Force interests. A flamlelet combustion sub-model [1] may be most appropriate for the flamelet regime, while a distributed reaction sub-model may be a better choice to simulate a high-swirl conditions in gas turbine and other types of engines [2]. Experiments have been needed to determine which modeling approach is most appropriate for each regime.

The flamelet approach of Pitsch, Moin, Ihme and others assumes that the profiles of species and temperature are broadened by the turbulence, but it may not account for the observation that preheat zones can be preferentially broadened when the reaction layers are not broadened. Another approach is the Partially Stirred Reaction (PaSR) model of Poinsot and colleagues that assumes that significant broadening of the reaction zone occurs; for certain conditions the experiments show that this assumption fails. The G-equation model [1] can fail when broken reaction layers occur since the model assumes the existence of a continuous reaction layer.

Some previous predictions of regime boundaries have been reported by Borghi [3, 4], Klimov and Williams [5, 6] and Peters [7, 8]. Klimov and Williams predicted that preheat layers are broadened when the Kolmogorov eddy size equals the preheat layer thickness. Peters predicted that broken reactions occur when the Kolmogorov eddy size equals the reaction layer thickness. He showed that this occurs when his Karlovitz number (the nondimensional strain rate) based on the Kolmogorov scale equals unity. Other studies have attempted to predict when distributed reactions occur [9, 10]. While these predictions sometimes have been accepted as being valid, it is unfortunate that there has been not been sufficient experimental evidence to assess if they are accurate or if they need to be modified. For example, just because a Kolmogorov eddy can fit inside a preheat zone does not guarantee that turbulent diffusion will dominate over molecular diffusion, which is required to cause significant broadening. Just because the Kolmogorov eddy fits inside the reaction zone does not insure that a broken reaction layer results. A Kolmogorov eddy is so weak that it cannot survive even one eddy rotation before it is dissipated by viscous forces. Eddies much stronger than the Kolmogorov eddies may be required to broaden the preheat zones and to break the reaction layer.

The present study is the second phase of a two-phase effort. The first phase was reported in a previous paper (PROCI) that described a methodology developed to determine the regime associated with each of five different cases. In that paper the regime boundaries could not be reported because five cases are insufficient and because the cases did not extend sufficiently into the broken reaction regime. Therefore the present paper includes (?) cases from which boundaries can be determined, and the cases now extend into the broken reaction regime.

To measure regime boundaries it was necessary to achieve a wide range of turbulence levels (u') and integral scales (λ_I) and to insure that both u' and λ_I are relatively uniform in space in the

reactant flow field upstream of the flame. To do so, a unique Hi-Pilot burner was designed to provide turbulence levels (u'/S_L) up to 160, which is four times that of previous studies. Integral scales were varied from 7 to 35 mm, which provides both high Reynolds and high Karlovitz numbers. Preheat and reaction layers were imaged using PLIF diagnostics that excited CH, as well simultaneous excitation of hydroxyl (OH) and formaldehyde.

It is noted that we cannot assume that the Borghi diagram is sufficient to understand and to plot all of the possible regimes of premixed turbulent combustion. The Borghi diagram only focuses on two parameters (u'/S_L) and ($\lambda_I / \delta_{F,L}$), which are defined in the Nomenclature. It may be necessary to add additional axes to the Borghi diagram to account for: (a) residence time of eddies in the flame, (b) the temperature of preheated reactants, (c) multiple Damkohler or Karlovitz numbers to account for auto-ignition and other types of chemistry, (d)… For example, residence time is important since the flame tip has reaction regions that are broader, broken and more distributed than at the flame base. Thus (x/U) is an additional parameter of importance. Spherical flames become more wrinkled as time progresses, so their properties cannot be captured by one point on a Borhgi diagram. Premixed flames also have some geometry dependence, so a separate Borghi diagram may be necessary for each general flame type (Bunsen, V-type, jet-type, spherical, counterflow).

Even after regime boundaries are measured, research still is needed to explain the physical reasons that cause transitions to different regimes. For example, broken flamelets may be a necessary precursor to distributed reactions. A continuous reaction layer directs products at high speeds away from the reactants. However, when local flame extinction creates holes in the reaction surface it may be possible for hot product to be convected upstream and mix with the reactants. Such mixing may lead to locally distributed reactions.

Previous predictions of regimes

Two interesting and unexplored areas on the Borghi diagram are at the upper right corner of Fig. 1 (large Reynolds number) and at the upper left corner (large Karlovitz number). Turbulent Reynolds number (Re_T) is defined a ($u' \lambda_I / \nu$). One commonly used Karlovitz numbers is based on the Kolmogorov length scale, as defined by Peters [7], while another is based on the integral length scale:

$$Ka_{Peters} = (\delta_{F,L} / \eta_K)^2 , \qquad Ka_{Integral} = (u'/\lambda_I)/(S_L^2/\alpha) \qquad (1a,b)$$

In the high Reynolds number region the turbulent diffusivity becomes large with respect to molecular diffusivity because both the turbulent diffusivity and Reynolds number are proportional to ($u' \lambda_I$). The eddies are sufficiently large and sufficiently strong to roll up the flame surface. It is believed that violent mixing of some hot products with reactants can occur, despite the fact that the flame tends to force hot products to move away from the flame surface at a speed that is typically 3-5 times S_L. A larger integral scale promotes local extinction, as was shown by the flame-vortex computations of Meneveau and Poinsot [11, 12] and the experiments of Roberts et al. [13]. Both studies showed that large eddies are more efficient at extinguishing a flame than small eddies. The reasons are not clear, but it is likely that local extinction requires that local strain rate is not the only criterion; to cause extinction the eddy rotational velocity should approximately equal or exceed the flame speed. It also might require a lifetime that is sufficiently long. These conditions are not met by the small eddies.

The quantities in Eq. 1 are defined in the Nomenclature. Therefore, if it is desired to operate in the upper right corner of Fig. 1, the integral scale should be made large, while to operate in the upper left corner the integral scale should be made small.

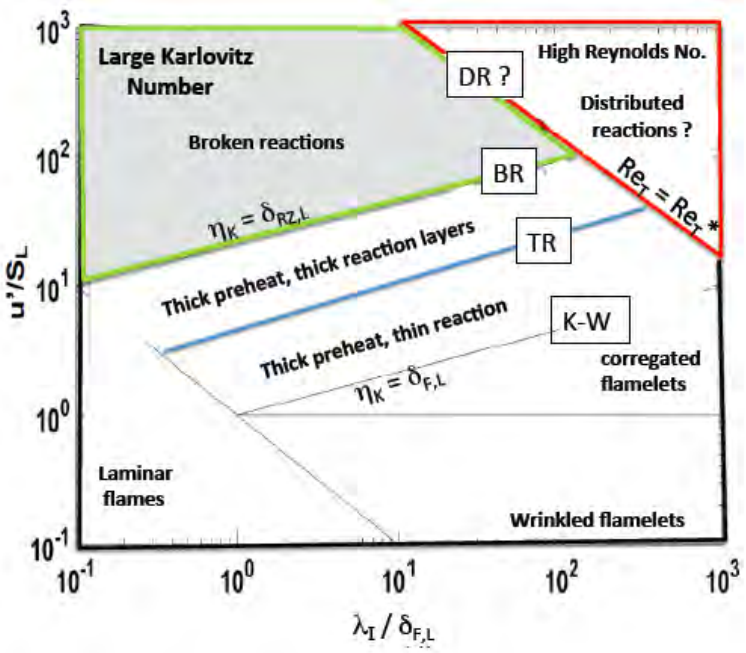

Figure 1. Two unexplored regimes on the Borghi diagram: the large Karlovitz region (upper left) and the high Reynolds number region (upper right). Four theoretical regime boundaries are labeled K-W (Klimov-Williams, thick preheat layers), TR (thick reaction layers), BR (broken reactions), DR (distributed reactions).

a) The TP (thickened preheat) regime and the Klimov-Williams boundary

The Klimov-Williams boundary [9] is marked K-W in Fig. 1. Kolmogorov eddies fit inside the flame thickness, so:

$$\eta_K = \delta_{F,L} \tag{2}$$

If the Kolmogorov scale in Eq. 3 is replaced by its definition: $c_2\ \lambda_I\ (Re_T)^{-3/4}$, then Eq. 3 can be rearranged to yield the following relation that shows that the K-W boundary has a slope of 1/3 on a log-log Borghi plot:

$$\frac{u\prime}{S_L} = c_4 \left(\frac{\lambda_I}{\delta_{F,L}}\right)^{1/3} \quad \text{Klimov-Williams boundary} \tag{3}$$

The constant c_3 is the molecular Schmidt number ($\nu/D = 0.8$).

b) The BR (broken reaction layer) boundary

The upper left portion of the Borghi diagram is the high Karlovitz region and it is labeled Broken Reactions. Karlovitz number (non-dimensional strain rate) is known to govern the extinction of laminar flames but it is not known, from experimental data, whether the appropriate

Karlovitz number is one base because Peters [4] predicted that broken reactions occur when a second type of Karlovitz number (that he defined to be Ka_δ) is unity; thus:

$$Ka_\delta = (\delta_{RZ,L} / \eta_K)^2 = 1 \quad \text{at the broken reaction (BR) boundary} \qquad (4)$$

It follows that at the predicted BR boundary the Kolmogorov eddies just fit inside the reaction layer. Replacing the Kolmogorov scale in Eq. 6 leads to:

$$\frac{u\prime}{S_L} = c_6 \left(\frac{\lambda_I}{\delta_{F,L}}\right)^{1/3} \quad \text{at the BR boundary} \qquad (5)$$

and $c_6 = c_5\, c_4^{-4/3}$. The constant c_4 is defined to be the ratio of laminar reaction zone thickness ($\delta_{RZ,L}$) to the laminar total flame thickness ($\delta_{F,L}$); it has the value of 0.1 based on CHEMKIN computations. The BR boundary predicted by Eq. 5 is plotted in Fig. 1. Equation 5 indicates that the predicted Broken Reaction boundary has a slope of 1/3 and has values of u'/S_L that are larger than those on the K-W boundary by a factor of $c_4^{-4/3}$ which is 22.

No previous measurements have been available to determine if broken reactions do occur above the predicted BR boundary. The theory assumes that going to very small integral scales (associated with large Ka_δ in the upper left of the Borghi diagram) is more likely to lead to broken reactions than by going to large integral scales. This assumption has not been experimentally assessed.

c) The DR (distributed reactions) boundary

A flamelet is defined to be a layer by Peters [7], so it must have one dimension that is sufficiently smaller (typically four times smaller) than its dimension in a perpendicular direction. In contrast, a distributed reaction region does not have one dimension that is (typically) four times smaller in any one direction, so it may look like an ellipse or be irregularly-shaped. There are three situations for which distributed reactions are known to occur. First, the rapid compression of reactants within a shock tube or an HCCI engine is known to rapidly elevate the temperature of the reactants above the ignition temperature, causing reactions to become distributed in space [4]. Alden et al. reported broad CH zones within an HCCI engine experiment. If instead there are some temperature inhomogeneities, there may be many ignition locations that create densely-packed flamelets; these are essentially distributed reactions.

The second way is to preheat the reactants to a temperature just below the ignition temperature and then inject them into a strong internal recirculation zone, along with some EGR (exhaust gas recirculation) gas. A"flameless" regime diagram that is a plot of preheat temperature versus internal recirculation zone strength. "Flameless" conditions are said to occur in the upper right corner of such a plot. However, the diagnostics that have been used to date to identify flameless combustion have not been adequate. The only diagnostics that can determine if reactions are distributed in space are CH PLIF, OH-formaldehyde PLIF or OH-HCO PLIF. It has been claimed that a region of uniform chemiluminescence is an indicator of flameless combustion. However, this is not proof that flamelets no longer exist; it could only indicate that there are products (including OH*, which emits chemiluminescence) and not distributed reactions.

A third way to create distributed reactions is by turbulence alone, without the help of preheating, internal recirculation, a piston or a shock wave. The small amount of evidence to date

indicates that turbulence alone does not create large, uniform reaction zones, but instead produces pockets of distributed reactions that are connected to each other by thin flamelets. This situation has been called "partially-distributed". We have shown that turbulence must be so intense that conditions first must lie above the broken reaction boundary before "partially-distributed" reactions occur. That is, the Karlovitz number required to break the flamelets appears to be smaller than the Karlovitz number required to create small, local distributed reaction regions. After holes in the flamelets are created, it appears that large integral scales are effective in mixing reactants and products, so that locally-distributed reactions occur above a critical turbulent Reynolds number.

There is no accepted theoretical criterion that adequately predicts the boundary of the distributed reaction regime. Peters [7] argues that $Ka_\delta = 1$ leads to broken reactions, and this may be a necessary but not sufficient criterion for distributed reactions. Holes in the flamelets may allow hot products to be convected upstream and mix rapidly with reactants. With no holes, the products are given a large velocity away from the flame, which is difficult to overcome by the small velocity within an eddy. Near a hole there is no flame-induced velocity. Thus the eddy may be able to rapidly mix hot products into the reactants and raise the temperature of the reactants within a very short time (Δt) to a temperature that exceeds the ignition temperature. If the time Δt is less than the ignition delay time (τ_{delay}) i.e.,:

$$\Delta t \leq \tau_{delay} \qquad (6)$$

then it should be possible for chemical reactions to begin at many locations and create a distributed reaction region. Several ways to achieve Eq. 6 are to create holes between broken reaction layers, to impose a strong recirculation zone, to preheat the reactants so that they are just below the ignition temperature. Other ways are to rapidly compress in a shock tube or an HCCI engine.

d) Two other important factors: residence time and reactant temperature

The Borghi diagram may give the erroneous impression that the various regimes are determined only by the two parameters (u'/S_L) and ($\lambda_I / \delta_{F,L}$). I While it is important to measure the regime boundaries, it cannot be assumed apriori that the Borghi diagram is an adequate way to plot the results. The Borghi diagram (turbulence intensity versus integral scale) is only one slice of a multi-dimensional map.

Results below indicate that other governing parameters are: residence time, reactivity (temperature of reactants relative to ignition temperature) and stratification of reactants or products. A different map may be required for each category of the geometry (Bunsen, jet, spherical, counterflow or V-flame) since each imposes different boundary conditions. The present approach is to measure the regime boundaries and then decide if the Borghi diagram remains useful. t is known that residence time is another parameter that is important. The tip of Bunsen flame is more wrinkled than at the base. Also, a spherical flame becomes progressively more wrinkled in time. These changes occur when the two parameters (u'/S_L) and ($\lambda_I / \delta_{F,L}$) are kept uniform in space and time upstream of the flame. Raising the initial temperature of the reactants is likely to affect all of the boundaries. Preheated reactants are closer to the ignition temperature and are more likely to form distributed reactions, based on Eq. 8. Preheating also increases the gas viscosity that can weaken the eddies as they pass through the preheat zone, causing eddies to

be too weak to disturb the reaction layer. The temperature of the reactants also affects the laminar burning velocity.

The flame thickness has been defined in several ways. ($\delta_{F,L}$) is the unstretched laminar flame thickness that is equal to the thermal thickness:

$$\delta_{F,L} = (T_2-T_1)/(dT/dx)_{max} = c_1 (D/S_L) \quad (2)$$

The constant c_1 is 8, based on CHEMKIN computations [5] for methane-air, ϕ = 0.75. The Kolmogorov scale is η_K , λ_I is the integral scale and D/S_L is called the Zeldovich flame thickness, where D is molecular diffusivity.

$$c_5 = \left[\frac{c_2^2\, c_3\, Ka^{2/3}}{c_1}\right] \quad (5)$$

Since Ka is defined to be unity at the theoretical K-W boundary, then using Eq. 5 the value of c_5 is calculated to be 0.25. While the Klimov-Williams relation (Eq. 4) is the predicted boundary of thick preheat zones, this relation has not been experimentally validated because measured values of the boundary previously have not been available. Even when Kolmogorov eddies can fit inside a preheat zone they may not be strong enough to thicken the preheat zone.

3. Previous experimental and DNS studies

Previously, Gülder and colleagues [14, 15] performed Rayleigh and OH PLIF imaging of premixed flames for the largest turbulence levels at that time. They achieved u'/S_L values as large as 24. The present work considers the new range of extreme turbulence, which we define to be values of u'/S_L between 24 and 243. Other relevant experiments are those of Refs. 16-34.

	Turbulent Reynolds No. $u' \lambda / \nu_o$	Senior author	Location	Burner type
High Re_t	5,000 - 80,000	Driscoll Hi-Pilot (present study)	Michigan	bunsen
Inter-mediate Re_t	2,000-5,000	Dunn, Masri [1]	Sydney	jet
		Alden [2]	Lund	jet
		Sweeney, Barlow [3]	Sandia	jet
		Shepherd, Cheng [4]	Berkeley LBL	lo-swirl
Low Re_t	under 2,000	Y. Ju [5]	Princeton	bunsen
		Chen, Bilger [6]	Sydney	bunsen
		Peters, Cheng [7]	Germany	lo-swirl
		Shepherd [8]	Berkeley	V-flame
		Gokalp [9]	Orleans	bunsen
		Dinkelacker [10-12]	Hannover	bunsen
		Kobayashi [13]	Japan	bunsen
		Gulder [14]	Toronto	bunsen
		Driscoll, Carter [15]	Michigan	bunsen
		Driscoll, Faeth [16]	Michigan	bunsen

Table 1. Previous studies that reported flame thickness measurements.

Table 1 lists four previous studies that report flame thickness for "intense turbulence" (u'/S_L) up to 24 and our work (u'/S_L from 24 to 243). Reynolds numbers are listed. In all of these studies the reactants initially are at room temperature. Preheat thicknesses were determined from Rayleigh scattering or formaldehyde PLIF; reaction zone thicknesses were determined from either CH, formaldehyde/OH overlap or HCO PLIF images.
There has been confusion because there are only two ways to identify distributed reactions: CH PLIF and OH-formaldehyde overlap diagnostics (or the related OH-HCO overlap. It is not possible to identify distributed reactions using OH PLIF alone, by chemiluminescence, by temperature imaging, or by single point measurements, as has been claimed in the past.

Dunn, Masri and co-workers [19], operated a piloted premixed jet flame at intermediate Reynolds numbers (between 2,000 and 5,000). It is normally not possible to plot data from jet flames on a Borghi diagram because values of u', λ_I and Re_T usually are too difficult to measure within the reactants just upstream of the flame brush. Also, in a jet flame these quantities vary by large amounts in the flow direction.

Zhao, Alden and colleagues [16] imaged flame structure that showed some level of broken or distributed reactions. Zhou et al. [16] observed distributed CH regions near the tip of their premixed jet flame. Sweeney et al. [21] studied a premixed jet flame for a Re_T that is approximately 5,000. Using Rayleigh scattering they found that their normalized preheat layer did not thicken significantly; its normalized thickness varied only from 1.2 to 2.0. Shepherd et al. [22] considered a relatively flat flame stabilized in a low-swirl burner. Their turbulence levels (u') and integral scales ahead of the flame were relatively uniform and were measured. They used Rayleigh scattering to show that preheat zone thicknesses were three times the laminar value. While the limited individual data points from the above studies are interesting, no previous study has reported a set of measured regime boundaries that were determined after varying u' and integral scale.

DNS studies of Aspden et al. [35], Blanquart et al. [36] and Sankaran et al. [37] were performed at large Karlovitz number that exceed 1500 by selecting very small integral scales of one mm. Thus their Reynolds numbers were very small. In all three DNS studies they observed broken reactions that can be attributed to the high strain rate.

Goals of the present study

The goal has been to extend our understanding of the new physics that occur at Reynolds numbers that are ten time larger than previously studied, for premixed turbulent flames. We also achieved Karlovitz numbers (strain rates) five times larger than previous experiments. To understand the physics, PLIF images of CH, OH and formaldehyde were recorded. The CH PLIF was recorded at a 10 kHz rate. The PLIF images showed the structure of the preheat and reaction zones. A goal has been to assess two previous predictions: the Klimov-Williams boundary and the Peters Broken Flamelet boundary. A goal has been to determine the role of other governing parameters including residence time and stratification of the reactants and the products.

Calibration of the diagnostics and definitions of reaction and preheat layers

The reaction and preheat zones were imaged using simultaneous OH and formaldehyde PLIF diagnostics that are described in the appendix. Standard Nd:YAG and dye lasers were operated at 282 nm and 355 nm respectively and fluorescence was collected by intensified, gated UV

sensitive cameras. The spatial resolution of the PLIF measurements is 0.2 mm, which is the binned pixel size as well as the measured thickness of the laser sheet. The reaction zone is determined by the Overlap method that was developed previously [24-26]. Overlap is defined to be the product of the OH and formaldehyde PLIF signals. Arrhenius kinetics requires that certain reactions (between OH and formaldehyde) must occur in the overlap region, but this is only one of several possible reaction layers. Reaction layer thickness is defined to be the full width at half maximum of the overlap region.

To assess this approach, calibration studies were conducted both with a laminar conical Bunsen flame and with CHEMKIN computations. Refs. 38 to 48 also showed that formaldehyde can be used as a marker of the preheat zone. The CHEMKIN profiles in Fig. 2 show that heat release rate profile falls nearly on top of the Overlap profile. It also shows that formaldehyde exists throughout the preheat zone because it diffuses upstream from the reaction zone at the same rate as the gas temperature. The leading edge of the preheat zone is defined to be where formaldehyde is 35% of its maximum, and CHEMKIN indicates that the gas temperature is 550 K. The trailing edge of the preheat zone is the where the reaction zone begins. The laminar calibration flame data showed that in the overlap region the product of the two PLIF signals was a Gaussian profile that had a peak value that was constant and continuous along the flame.

The reaction zone was identified by recording the product of the OH and formaldehyde PLIF signals. To assess this approach calibration studies were conducted with a laminar conical Bunsen flame, and related computation were performed using CHEMKIN. Figure 3 shows the profiles that were computed using CHEMKIN for the same fuel and equivalence ratio as the turbulent flame experiment (methane at ϕ = 0.75). Notice that formaldehyde (CH_2O) exists throughout the preheat zone although it is not formed there. Formaldehyde is formed in the reaction zone by reactions between the methyl radical (CH_3) and O_2 (as well as other oxygen-containing species) and it then diffuses upstream at about the same rate as the gas temperature. Li et al. [38] showed that CH_2O can also be used as a marker of the preheat zone. The leading edge of the preheat zone was defined to be where formaldehyde signal is 25% of its maximum value because CHEMKIN shows that at this location the gas temperature is 550 K. The downstream edge of the preheat zone is defined to be the upstream edge of the reaction zone.

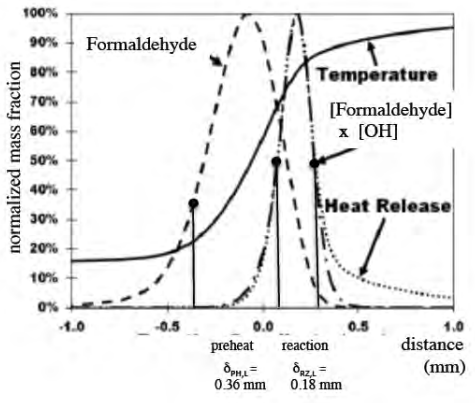

Figure 2. CHEMKIN laminar flame computations showing that formaldehyde marks the preheat zone while the overlap of formaldehyde-OH signal marks the reaction zone. Vertical lines mark preheat and reaction zones. Methane, equivalence ratio = 0.75. Flame thickness $\delta_{F,L}$ is 0.54 mm.

The reaction zone is defined to be the region where the product of the formaldehyde-OH signal exceeds 50% of its maximum value. This threshold level of 50% was selected because it is sufficiently larger than the background noise. This definition is consistent with many previous studies that defined the reaction zone to occur where there is overlap of OH and formaldehyde (or HCO) signals. Of course, there are many other reactions besides the formaldehyde-OH reaction; however, Fig. 4 shows that the profile of total heat release rate very closely overlaps the product of formaldehyde and OH. The thickness of a laminar flamelet ($\delta_{F,L}$) is defined to be the sum of the preheat thickness ($\delta_{PH,L}$) and the reaction zone thickness ($\delta_{RZ,L}$). The value of ($\delta_{PH,L}$) computed by CHEMKIN was 0.36 mm, which was used to normalize all of the present measurements.

The laser PLIF diagnostics are described in the Appendix. Simultaneous formaldehyde-OH PLIF images were acquired by overlapping two laser sheets having wavelengths of 355 nm and 282 nm. The spatial resolution of the PLIF measurements is 0.2 mm. This is the thickness of the laser sheet, as measured using a traversing razor blade. The pixels in the images were binned 4 pixels by 4 pixels so that the spatial resolution in the plane of the laser sheet also equals 0.2 mm. This level of binning provides a typical signal-to-noise ratio (S/N) of 15 for formaldehyde and for OH. Noise was measured using the laminar calibration flame; in a laminar, uniform region of OH or formaldehyde there should be no variations due to turbulence so the r.m.s. fluctuations measured in those regions are defined to be noise.

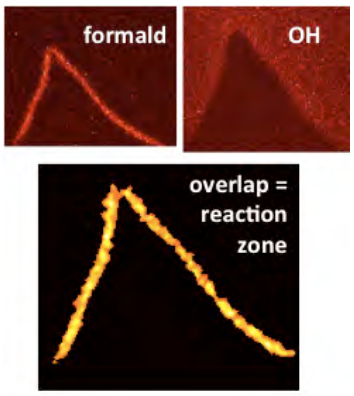

Figure 3. Laminar premixed calibration flame; PLIF images of formaldehyde, OH and overlap

A calibration experiment was run to assess the above definitions and the accuracy of the diagnostics. A laminar, lean premixed conical Bunsen flame was stabilized above a circular tube of diameter 10 mm. PLIF images of the formaldehyde and OH signals are shown in Fig. 1, along with an image of the product of the two signals. It is seen that the signal to noise is sufficient such that the image of the reaction zone is continuous, which is correct since the observed chemiluminescence is continuous. The measured thicknesses of the preheat and reaction zones are somewhat larger than the CHEMKIN computations because of two reasons. A calibration experiment was run to assess the above definitions and the accuracy of the diagnostics. A laminar, lean premixed conical Bunsen flame was stabilized above a circular tube of diameter 10 mm. PLIF images of the formaldehyde and OH signals are shown in Fig. 1, along with an image of the product of the two signals

It is seen that the signal to noise is sufficient such that the image of the reaction zone is continuous, which is correct since the observed chemiluminescence is continuous. The measured thicknesses of the preheat and reaction zones are somewhat larger than the CHEMKIN

computations because of two reasons. The spatial resolution of the diagnostics is 0.2 mm; this is more than sufficient for the highly turbulent flames of interest, but it is about equal to the thickness of the reaction zone of the laminar flame. A second reason is that the formaldehyde chemistry in CHEMKIN has some uncertainties. The formaldehyde chemistry is adequate to allow CHEMKIN to predict an accurate flame speed and an accurate ignition delay time. It is not known how accurately it can predict the thickness of the formaldehyde-OH profiles.

Michigan Hi-Pilot Burner and Operating Conditions

The Michigan Hi-Pilot Burner [48] in Fig. 3 is a piloted Bunsen burner that is designed to achieve very large values of u/S_L, integral scale, and Reynolds numbers, along with a uniform profile of turbulence levels and integral scales across the base of the flame. Reactants issue at mean velocities up to 110 m/s from the central burner that is 21.6 mm in diameter. The conical

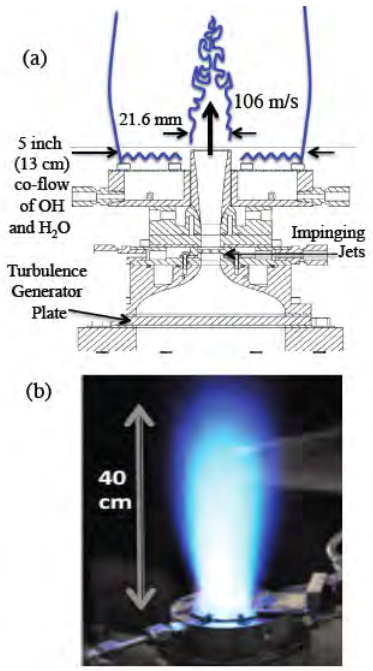

Figure 4. Hi-Pilot Burner designed and operated at the University of Michigan

premixed flame is located near the downstream edge of the jet core that has a height of about 6 burner diameters (126 mm). In this 126 mm tall jet core, turbulence levels and integral scales are relatively constant. The turbulence generator [49] consists of a slotted plate upstream of a converging nozzle. The longitudinal integral scales were measured by a laser velocimeter; integral scales first were measured in a pipe flow and were found to agree with published values.

All of the turbulent flames investigated in this paper were produced by the Michigan Hi-Pilot Burner. It is a piloted Bunsen burner that is designed to achieve high Reynolds numbers along with turbulence levels and integral scales that are relatively uniform in space upstream of a premixed flame. Details of the burner dimensions are given in Ref. 44. Reactants issue at mean velocities up to 110 m/s from the central burner that is 21.6 mm in diameter. The conical premixed flame is designed to be located near the downstream edge of the jet core of the central stream. The jet core has a height of about 6 burner diameters (126 mm). In this 126 mm tall jet

core, turbulence levels and integral scales are relatively constant in space, as is shown by LDV data plotted in Fig. 6. Values of u' are seen to be very uniform in the radial direction over a 20 mm region, which is 80% of the burner exit diameter. Having spatially uniform values of u' and λ_I avoids ambiguities that plague other burner geometries; for example, in a jet flame the turbulence level decays rapidly in the downstream direction all along the flame.

A specially-designed turbulence generator consists of a slotted plate that is upstream of a rapid reduction in the flow area. To vary the integral scale, slotted plates with different slot geometries were inserted. Impinging jets of reactants were added to increase the turbulent level. The burner has diverging walls that produce gas velocities that decrease in the downstream direction, in order to prevent flashback. Flow controllers were adjusted using a LabView control program. The pilot flame is shown in Fig. 4 to consist of a hydrogen-air premixed flame (ϕ = 0.8) that was stabilized above a 127 mm diameter grid. The pilot flame produces a co-flow of hot products that prevents cold ambient air from interacting with the flame. The co-flow is carbon-free to prevent it from forming any formaldehyde.

The operating conditions on centerline at the burner exit are listed in Table 2. To achieve the highest turbulent Reynolds number of 99,000 the mean velocity for Case 6a was set to 78 m/s so that u' becomes 37 m/s. The longitudinal integral scale was measured by a laser velocimeter to be 41 mm. To assess the accuracy of these values, measurements were regularly repeated in air that exits a pipe at the same mean velocity as the Hi-Pilot burner. In all cases the turbulent pipe flow has a 5% to 7% turbulence level and a longitudinal integral scale that is about 80% of the pipe radius, which is consistent with previous pipe flow studies [51]. The LDV sample size typically was 500,000.

Case	ϕ	U_0 (m/s)	u' (m/s)	λ_I (mm)	Re_T	Da_T	Ka_T	u'/S_L	$\lambda/\delta_{PH,L}$
2a	1.05	14	2.9	7.5	1,400	25.4	4.7	7.5	31
3a	1.05	32	6.0	20	7,900	33.1	8.5	15	84
4a	1.05	44	10	25	17,000	24.6	16.5	26	105
5a	1.05	64	24	37	58,000	15.1	50.4	62	154
6a	0.65	78	37	41	99,000	1.7	503	243	83

Table 2. Typical operating conditions for the Hi-Pilot burner. For all cases methane-air combustion (ϕ 0.75) occurs at reactant temperature of 296 K and pressure of 1 atm. S_L is 23.2 cm/s and $\delta_{PH,L}$ is 0.36 mm, as computed by CHEMKIN. U_0 is the centerline velocity 5 mm above the burner; other quantities are defined in the nomenclature and the text.

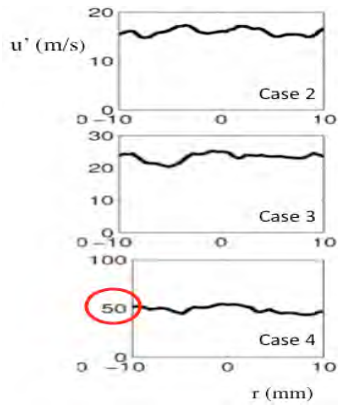

Figure 5. Turbulence level profiles at Hi-Pilot burner exit.

A laser velocimeter (described in the Appendix) was used to determine turbulence level and integral scales 5 mm downstream of the burner exit. The autocorrelation functions that are plotted in Fig. 6 were computed from the LDV data using the slotting method of Mayo et al. [52, 53]. Note that LDV measurements provide an integral *time* scale (τ), which is commonly converted to a length scale using Taylor's "frozen turbulence" hypothesis that states that integral length scale (λ_I) is $U_0\tau$. This hypothesis is accurate for small turbulent fluctuations (u'< 0.2 U), but for larger fluctuations Wu and Patterson [54] suggest that an additional term be included. This was done, so that:

$$\lambda_I = U_0\tau \ [1 + 5\ (u'/U)]^{1/2} \qquad (12)$$

For a typical turbulence intensity listed in Table 2, the quantity in the square brackets increases the integral scale by 65%.

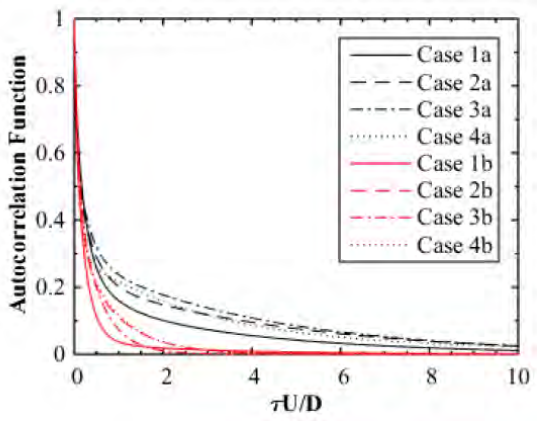

Figure 6. Typical autocorrelation functions from LDV that yield integral scales.

Results - Preheat zones - thickness and structure for intense turbulence (u'/S_L) up to 184

Figure 7 shows the instantaneous preheat zones in the Hi-pilot burner for Cases 1a-4a. The preheat zone is defined to start where the formaldehyde PLIF signal is 35% of its maximum value and it ends at the reaction zone, where the product of formaldehyde and OH PLIF signals is 50% of its maximum value. Case 1 represents the lowest turbulence level (u'/S_L = 6) considered; Re_t is 1,600. The preheat layers in Fig. 7a are continuous and have a thickness that is 2-3 times the laminar value of 0.36 mm. The preheat layers are highly wrinkled and form cusps and pockets. Results are similar to previously measured preheat layer properties [11-14] at similar low turbulence levels. It is concluded that Case 1 lies in the corregated flamelet regime.

It is surprising to see the extremely thick preheat zones in Figs. 7c and 7d that correspond to u'/S_L of 86 and 184 (Re_t is 40,000 and 80,000) respectively. To the authors' knowledge, preheat zones this thick have not been measured before. The arrows in Fig. 7d identify a preheat thickness of 25 mm, which is 70 times the laminar value. The theory of turbulent premixed flames predicts that the normalized thickness of the turbulent preheat zone ($\delta_{PH,T}/\ \delta_{PH,L}$) is proportional to the

square root of the ratio of turbulent to molecular thermal diffusivity (α_T / α), which should approximately be $(Re_T)^{1/2}$.

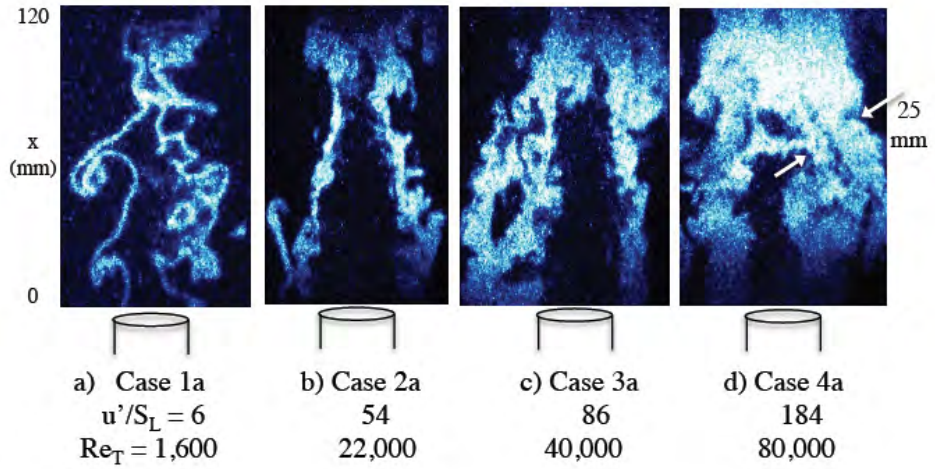

Figure 7. Preheat zone instantaneous images for Re_t from 1,600 to 80,000. Formaldehyde PLIF images are shown. Arrows indicate a preheat zone that is more than ten times thicker than the laminar value $\delta_{PH,L}$= 0.36 mm.

The blue regions (of formaldehyde signal) in Figure 7 show that the preheat zone thickness tends to increase with increasing turbulence intensity. Additionally, Figure 7 also indicates that the preheat zone thickness increases with height above burner. For heights greater than 20 mm above the burner, formaldehyde is found throughout the entire central region of the flame. Average thicknesses were measured by fitting a skeleton line that runs along each layer, halfway between the two edges. The distance between inner and outer boundaries is measured along the line that is normal to the skeleton. Normalized preheat zone thicknesses in Fig. 5 is as large as ten. "Thickened" preheat zones are defined to be normalized preheat thicknesses that exceed two.

Average values of preheat zone thicknesses first were determined for images of the flame "base" region (5 mm < x < 18 mm) for each case listed in Table 2. Typically 12,500 instantaneous thicknesses were averaged that represent 50 locations in 250 PLIF images. This averaging then was repeated for 12,500 locations within images of the flame "tip" region (20 mm < x < 33 mm). Figure 8 shows that the preheat zone thickness increases with the turbulence Reynolds number. However, the linear trend displayed by the results in Figure 14 suggest that the average preheat zone thickness is roughly a logarithmic function of Re_T, and hence possesses That is, the average preheat zone thicknesses level off for Re_T > 6,400. This asymptotic behavior makes sense because the area encapsulated by the flame brush is finite and for cases in which Re_T > 22,000 the preheat zone is seen to fill the entire central region of the flame Furthermore, comparing the results from the lower and upper zones in Figure 14, it is apparent that the average preheat zone thickness increases with height above burner.

An increase in preheat zone thickness with height above burner can be associated with the fact that the flame brush typically widens downstream of the burner's exit, which is a consequence of the burner's diverging nozzle. Additionally, this trend could potentially be attributed to elevated turbulence levels at moderate heights above the burner, which were observed in similar jet

burners. However, in order to validate this hypothesis, characteristics of the Hi-Pilot flow field must be assessed at regions downstream of its exit.

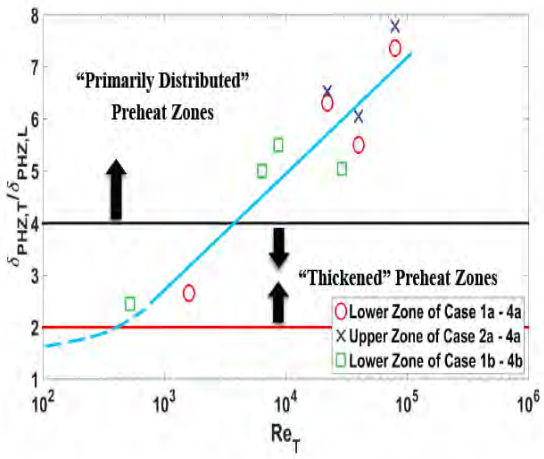

Figure 8. Average preheat zone thickness normalized by the laminar preheat zone thickness as computed in Chemkin (0.36 mm) as a function of Re_T.

The red horizontal line in Figure 8 marks the boundary between laminar and "thickened" preheat zones. The inequality defining this boundary is as follows:

$$4 > \frac{\delta_{PH,T}}{\delta_{PH,L}} > 2 \qquad (13)$$

Thus preheat zones that are more than two but less than four times as thick as those found in a laminar flame are identified as being "thickened." The boundary between "thickened" and "primarily distributed" preheat layers is marked by the black horizontal line in Figure 8. This boundary is defined by the inequality:

$$\frac{\delta_{PH,T}}{\delta_{PH,L}} > 4 \qquad (14)$$

(b) Reaction zones - thickness and structure for intense turbulence (u'/S_L) up to 184

The reaction zone was defined in Figure 2 as distance between locations where the product of the OH and formaldehyde PLIF signals is 50% of it maximum value. Figures 9a and 9b show instantaneous OH and formaldehyde PLIF images in the flame tip region of Case 2. Fig. 8c is the product of the two previous images; a threshold is applied to make pixels black if their value is less than 50% of the maximum value. A commercial image analysis code creates a skeleton line in Fig. 8d that is halfway between the edges of the reaction zone. Thickness is the distance between the edges of the reaction layers, along lines that are perpendicular to the skeleton line

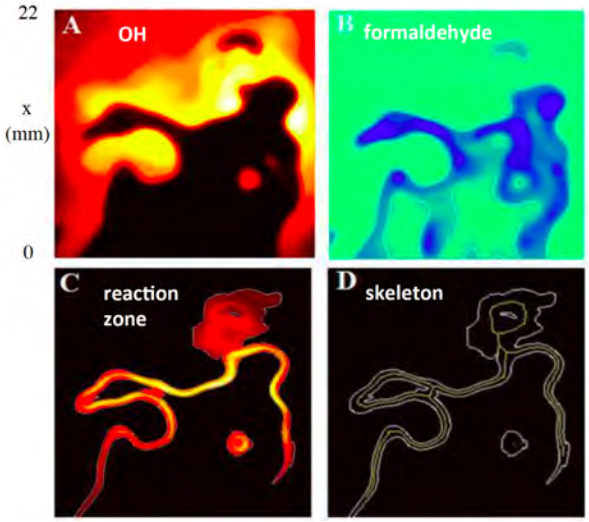

Figure 9. Instantaneous PLIF images of (a) OH, (b) formaldehyde, (c) reaction zone (overlap of OH-formaldehyde) and (c) skeleton, showing lines halfway between the edges of the reaction zone

Fig. 10 is a collection of individual images that were taken at random times at different locations. Near the flame base the reaction zones are thin layers (only twice the laminar thickness), while near the flame tip the layers are seen to be about four times the laminar thickness. There is significant large-scale wrinkling observed, but there is no evidence of broken or distributed reactions. Magnified images are reported in Figs. 11-15 at the two locations marked in Fig. 11. These higher resolution images emphasize the patterns seen in Figure 10. That is, the preheat zone thickness increases with increasing turbulence intensity while the reaction zone layers take on a variety of shapes. Specifically, while images taken from the lower zone of case 1b (shown in Figure 11) exhibit preheat zones that are only slightly larger than the reaction zones, images from the upper zone of case 4a (shown in Figure 13) show preheat zones that completely fill the flame brush. As alluded to above, unlike the preheat zones, trends associated with the reaction zones cannot be easily extracted from Figures 10 – 13. Take for example case 1b, which was the least turbulent case considered and, based on its boundary conditions, is classified into the "thin reaction zone" regime (see Figure 1). Nevertheless, Figures 10B and 10C clearly show that it is possible for this case's reaction zones to become thick and distributed. On the other hand, case 4a was the most turbulent case considered and, according to its measured boundary conditions, falls into the "distributed reaction zone" regime (see Figure 1). Yet, relatively thin reaction zone structures are observed in Figures 14a and 14c. Additionally, Figures 12 and 13 demonstrate that both thick and thin reaction regions exist within moderately turbulent flow fields. The fact that each case exhibits a mixture of thin and distributed reaction zones leads to average reaction zone thicknesses that vary only slightly with large increases in u'/S_L, Re_T, Da_T, and Ka_T.

In contrast to the preheat zone, trends associated with the reaction zone thickness are more difficult to extract from Figure 8. This is because segments of both thick and relatively thin reaction zones can be seen throughout the entire field in each of the four images.

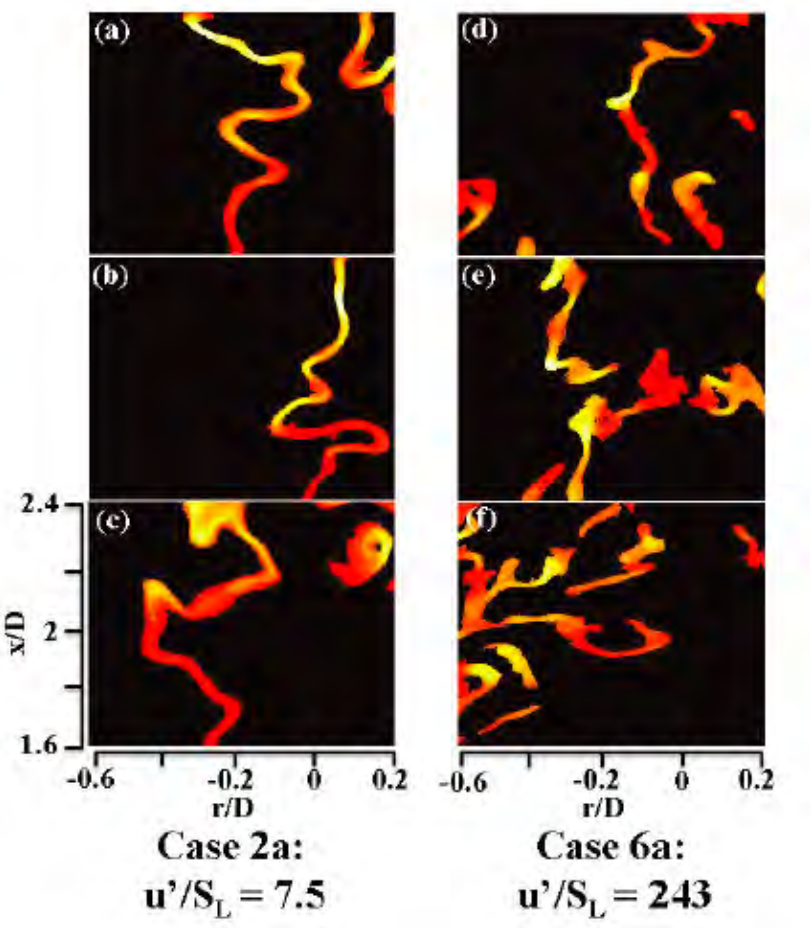

Figure 10. Reaction zones instantaneous images at random times for Case 2a and Case 6a.

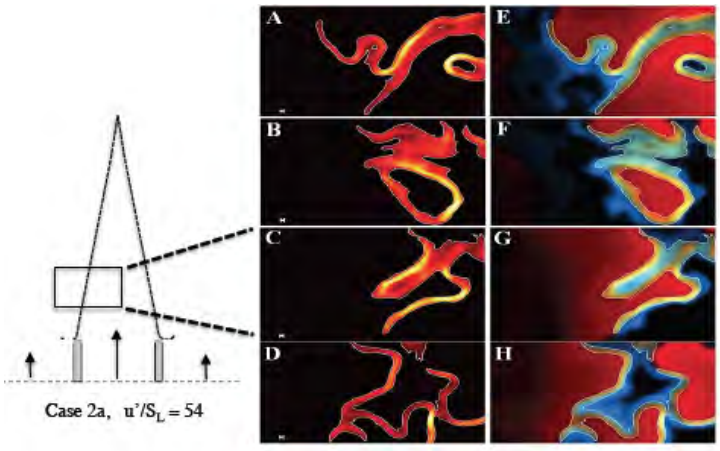

Figure 11. Reactions zones for the case 2b flame base region, at four random times: panels (A) – (D). Panels (E)-(F) display the preheat zone (blue = formaldehyde), product gases (red = OH signal) and reaction zone (yellow)

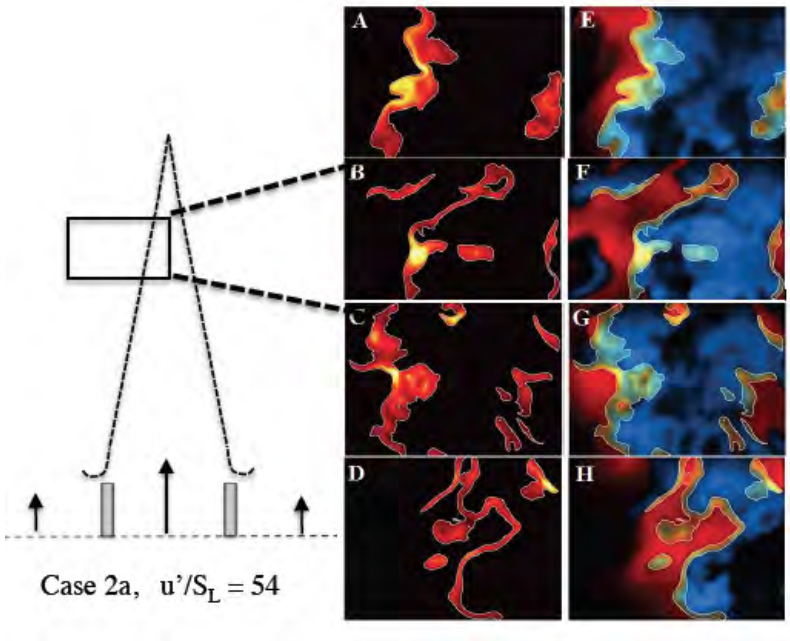

Figure 13. Reactions zones for the case 2b ($u'/S_L = 42$) flame tip region. Panels (A) – (D) were recorded at four random times. Panels (E)-(F) display the preheat zone (blue = formaldehyde), product gases (red = OH signal) and reaction zone (yellow). Field of view is 13 mm x 20 mm.

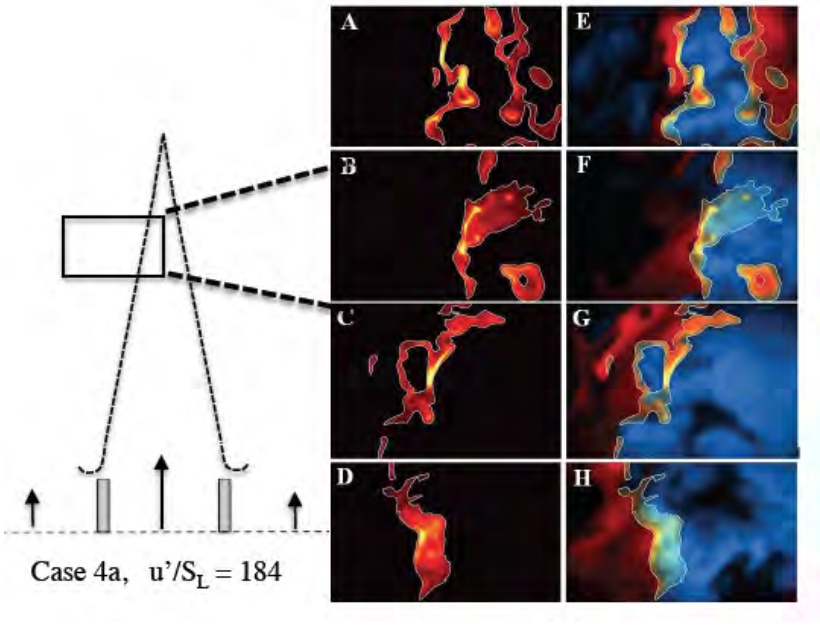

Figure 14. Additional reactions zone images for the case 2b ($u'/S_L = 184$) flame tip region. Panels (A) – (D) were recorded at four random times. Panels (E)-(F) display the preheat zone (blue =

formaldehyde), product gases (red = OH signal) and reaction zone (yellow). Field of view is 13 mm x 20 mm.

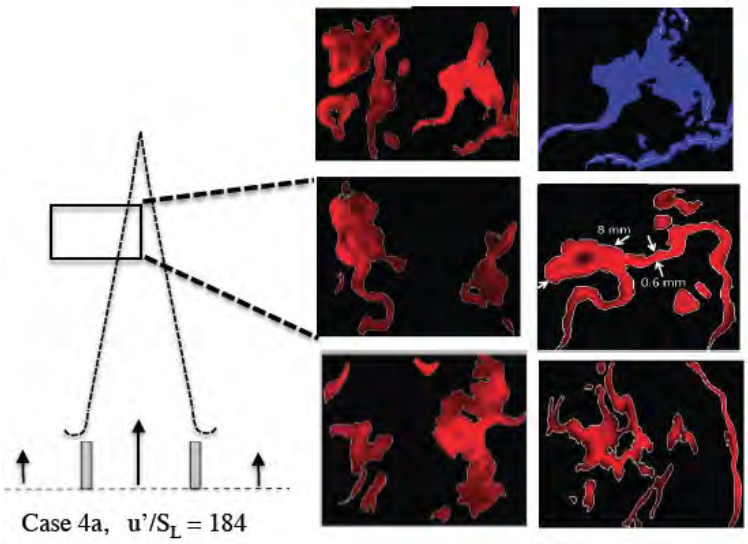

Figure 15. Selected images of distributed reactions for case 6b (u'/S_L = 184) flame tip region. Panels were recorded at random times. Field of view is 13 mm x 20 mm.

Figure 16 displays the average reaction zone thickness; each measurment was determined by fitting a skeleton and measuring the distance between inner and outer boundaries along a line normal to the skeleton. Each data point represents the average of 12,500 instantaneous thicknesses determined at typically 50 locations in each of 250 images.

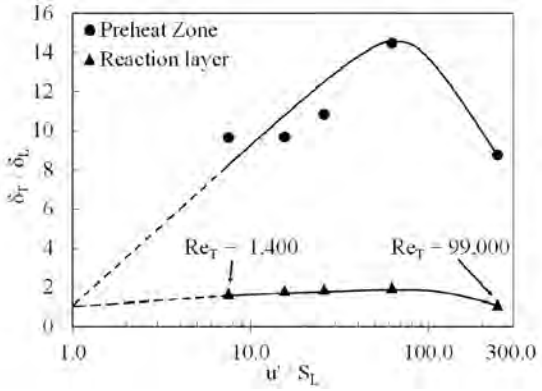

Figure 16. Average reaction zone thickness as a function of turbulence Reynolds number. Results are normalized by the laminar reaction zone thickness of 0.18 mm as computed by CHEMKIN

Unlike the average preheat zone thicknesses; Figure 16 implies that the average reaction zone thicknesses are relatively constant for a large range of turbulence intensities and integral length scales. This trend, or lack thereof, is consistent with the structural qualities of the reaction zones seen in Figures 10 – 13. Namely, while regions of distributed reactions were observed in cases with both high and low turbulence levels; they typically were also accompanied by relatively thin reaction regions. Having both relatively thin and distributed reaction layers present in all of the cases is what leads to minor variation between the average reaction zone thicknesses.

Conclusions

a. **Premixed turbulent flames were operated in the new regime** of extreme turbulence (u'/S_L) that varied between 24 and 243. Previous work has been reported for "intense turbulence" values of (u'/S_L) up to 24. Integral scale was varied from 6 to 30 mm. Karlovitz number was 139 and turbulent Reynolds number was as large as 100,000.

b. **A new Hi-Pilot burner** provides large turbulence levels and integral scales that are relatively uniform upstream of the flame. The OH-formaldehyde PLIF diagnostics first were applied to a laminar calibration flame and were found to yield flame thicknesses that agreed with CHEMKIN computations. The thicknesses and structure of both the preheat and reaction zones were measured for eleven cases using CH PLIF and simultaneous OH and formaldehyde PLIF. The PLIF diagnostics first were applied to a laminar calibration flame to compare flame thickness with CHEMKIN computations.

c. **Preheat zone average thickness** was found to exceed seven times the laminar value in the new range of extreme turbulence, which is much larger than previously observed. The curve of preheat zone thickness leveled off and became insensitive to turbulence level.

d. **Reaction zone average thickness** did not increase appreciably above the the laminar reaction zone thickness. One possible explanation for the difference is that after eddies broaden the preheat zone, they no longer can reach the reaction zone due to viscous decay.

e. **Residence time** of eddies in the flame brush was found to be an important parameter. The thickness of preheat and reaction zones both increase with (x/U) even though both locations experience about the same incident turbulence level and integral scale. This implies that the non-dimensional residence time $(x/U) / (\lambda/\nu)$ is a parameter should be included as an additional axis to the Borghi diagram.

f. **"Partially-distributed" reaction zones** were observed that contain up to 20% distributed reaction zones with the remainder being thickened layers.. A distributed zone is defined in Table 5 to have a longest dimension that does not exceed four times its shortest dimension, so it is not layer-like. No conditions were found to have 100% distributed reactions.

g. **"Distributed flamelets**" are a new phenomenon that appeared only at the largest turbulence intensities provided in this study. The CH layers remained thin but were extremely wrinkled into a "fractal-like" pattern such that most of an entire region in space was undergoing chemical reactions.

h. **The extent of the "thickened flamelet" regime** is larger than previously predicted, since several conditions that are found to have thickened flamelets lie outside the predicted boundaries. A cautious approach is to assume that the present results apply only to piloted Bunsen flames until additional measurements are reported for other flame geometries.

i. **The degree of stratification of the products** was found to be another parameter of importance. Stratification of hot products is due to outside air is entrained into the products.

Acknowledgements

Support for this research was provided by AFOSR Grant FA9550-12-1- 0101 that was monitored by Dr. Chiping Li.

References

1. Knudsen, E. and Pitsch, H., Combustion and Flame 159 (2012) 242–264.
2. Kodavasal, J., McNenly, M. J., Babajimopoulos, A., Aceves, SM, Assanis, DN, Havstad, MA, Flowers, DL, Int. J. of Engine Research 14, 5 (2013) 416-433.
3. R. Borghi, 1985, On the structure and morphology of turbulent premixed flames. In C. Casci (Ed.), Recent Advances in the Aerospace Sciences (New York: Plenum Publishing Corporation), pp. 117–138.
4. R. Borghi, Prog. Energy Combust. Sci. 14 (4) (1988) 245-292.
5. F. A. Williams, Combust. Flame 26 (1976) 269-276.
6. Kuo, K.K. Combustion Theory, Addison Wesley, Pub. 2002.
7. N. Peters, Turbulent Combustion, Cambridge U. Press, Cambridge UK, 2000.
8. N. Peters, N., 1999, The turbulent burning velocity for large scale and small scale turbulence. Journal of Fluid Mechanics, 384, 107–132.
9. Abdel-Gayed, R.G., Bradley, D. and Lung, F.K.-K., 1989, Combustion regimes and the straining of turbulent premixed flames. Combustion and Flame, 76, 213–218.
10. Lipatnikov, A.N. and Chomiak, J., 2002, Turbulent flame speed and thickness: phenomenology, evaluation, and application in multi-dimensional simulations. Progress in Energy and Combustion Science, 28, 1–74.
11. Veynante D., and Duclos, F., Proc. Combust. Inst. 32, 267 (2009)
12. Meneveau C, Poinsot T. , Stretching and quenching of flamelets in premixed turbulent combustion. Combust Flame 1991;86:311–32. Peters, N., 2000, Turbulent Combustion (Cambridge, UK: Cambridge University Press).
13. Poinsot, T. and Veynante, D., 2001, Theoretical and Numerical Combustion (Flourtown, USA: R.T. Edwards).
14. Roberts WL, Driscoll JF, Drake MC, Goss LP. Images of the quenching of a flame by a vortex—to quantify regimes of turbulent combustion. Combust Flame 1993; 94:58–69.
15. Pitsch, H. and Duchamp de Lageneste, L., 2002, Large–eddy simulation of premixed turbulent combustion using a level–set approach. Proc. of the Combustion Institute, 29, 2001–2008
16. M. Düsing; A. Sadiki; J. Janicka, Towards a classification of models for the numerical simulation of premixed combustion based on a generalized regime diagram, Combustion Theory and Modelling, Vol. 10, No. 1, February 2006, 105–132
17. R. J. Kee, Rupley FM, Miller JA, CHEMKIN, Sandia National Laboratories Report No. SAND 89-8009B, Livermore, CA; 1989.
18. Damkohler G., Jahrb. deut. Luftfahrtforsch, Z. Electrochem. 46, (1940) p.113. Also see Lewis B, von Elbe G. Combustion, flames and explosions of gases. New York: Academic Press; 1961.
19. Donzis, D. A, Sreenivasan, K.R., The bottleneck effect and the Kolmogorov constant in

isotropic turbulence, J. Fluid Mech. 657, 171-188, 2010.
20. B. Zhou, C. Brackmann, Q. Li, Z. Wang, P. Petersson, Z. Li, M. Alden, X. Bai, Combustion & Flame, 162 (2015) 2937-2953.
21. M.J. Dunn, A. R. Masri, R. W. Bilger, R S. Barlow, Flow Turbulence Combust. 85 (2010) 621–648.
22. Cavaliere, A., de Joannon, M., Mild Combustion, Progress in Energy and Combustion Science 30 (2004) 329–366.
23. M.J. Dunn, A. R. Masri, R. W. Bilger, R.S. Barlow, G.S. Wang, Proc. Combust. Inst. 32 (2009) 1779–1786.
24. B. Zhou, C. Brackmann, Z. Li, M. Alden, X. Bai, Combust. Inst. 35 (2015) 1409 – 1416.
25. M. S. Sweeney, S. Hochgreb, M. J. Dunn, R. S. Barlow Combust.Flame 159 (2012) 2896–2911.
26. I.G. Shepherd, R. K. Cheng, Combust. Flame 127 (2001) 2066-2075.
27. S.H Won, B. Windom, B. Jiang, Y. Ju, The role of low temperature fuel chemistry on turbulent flame propagation, Combustion and Flame 161 (2014) 475–483
28. Y.-C. Chen, R. W. Bilger, Combust. Flame 131(2002) 400–435.
29. Mansour, M.S. Chen, Y.-C., Peters, N., Proc. Combust. Inst. 24 (1992) 461-468.
30. I.G. Shepherd, R. K. Cheng, Combust. Flame 127 (2001) 2066-2075.
31. Lachaux T, Halter F, Chauveau C, Gokalp I, Shepherd IG. Flame front analysis of high pressure turbulent lean premixed methane air flames. Proc Combust Inst 2005;30:819–26.
32. A. Buschmann, F. Dinkelacker, T. Schafer, M. Schafer, J. Wolfrum, J.. *Proc Combust. Inst*. 26 (1996) 437–445.
33. A. Soika, F. Dinkelacker, A. Leipertz, *Proc. Combust. Inst* . 27 (1998) 785–792.
34. H. Kobayashi, T. Kawahata, K. Seyama, T. Fujimari, J.S. Kim, *Proc. Combust. Inst.* 29 (2002) 1793-1800.
35. F.T.C. Yuen, O. L. Gulder, *Proc. Combust. Inst. 34* (2013) 1393-1400. Also: see F.T.C. Yuen, O. L. Gulder, Comb. Sci. Technol. 182, 544-558, 2010.
36. S.A. Filatyev, J.F. Driscoll, C. D. Carter, J. M. Donbar, Combust. Flame 141 (2005) 1–21.
37. J. F. Driscoll, *Prog. Energy & Combust. Sci.* 34 (2008) 91-134.
38. Ratner A, Driscoll JF, Donbar JM, Carter CD, Mullin JA. Reaction zone structure of nonpremixed turbulent flames in the intensely wrinkled regime. Proc Combust Inst 2000; 28:245–51.
39. W. Meier, X.R. Duan, P. Weigand, Reaction zone structures and mixing characteristics of partially premixed swirling CH4/air flames in a gas turbine model combustor, Proceedings of the Combustion Institute 30 (2005) 835–842
40. A. J. Aspden, M. S. Day, J. B. Bell, *J. Fluid Mech.* 680 (2011) 287–320.
41. B. Savard, B. Bobbitt, G. Blanquart, Structure of a high Karlovitz premixed turbulent flame, Proceedings of the Combustion Institute 35, 2, 2015,1377–1384.
42. J. B. Bell, M.S. Day, J. F. Grcar, M.J. Lijewski, J. F. Driscoll, S. Filatyev, *Proc. Combust. Inst.* 31 (2007) 1299–1307.
43. R. Sankaran, E.R. Hawkes, J.H. Chen, JH., Proc, Combust, Inst, 31(2006)1291–1298.
44. Z. Li, B. Li, Z. Sun, X. Bai, M. Alden, Combustion and Flame 157 (2010) 1087-1096.

45. M. Richter, R. Collin, J. Nygren, M. Alden, L. Hildingsson, B. Johansson, Studies of the Combustion Process with Simultaneous Formaldehyde and OH PLIF in a Direct-Injected HCCI Engine, JSME International Journal, Series B, Vol 48, No. 4, 2005.
46. B.O. Ayoola, R. Balachandran, J.H. Frank, E. Mastorakos, C.F. Kaminski, Combust. Flame 144 (2006) 1–16.
47. J. Kariuki, A. Dowlut, R. Yuan, R. Balachandran, Proc. Combust. Inst. 35 (2015) 1443-1450.
48. J. E. Temme, P.M. Allison, J. F. Driscoll, Combustion Instability of a Lean Premixed Prevaporized Gas Turbine Combustor Studied Using Phase-Averaged PIV, Combustion and Flame 161 (2014) 958–970.
49. S. Böckle, J. Kazenwadel, T. Kunzelmann, D-I. Shin, C. Schulz, J. Wolfrum. Proc. Combust. Inst. 28 (2000) 279-286
50. M. Röder, T. Dreier, C. Schulz, Applied Physics B 107 (2012) 611-617.
51. M. Röder, T. Dreier, C. Schulz, Proc. Combust. Inst. 34 (2013) 3549-3556.
52. B.O. Ayoola, R. Balachandran, J.H. Frank, E. Mastorakos, C.F. Kaminski, Combust. Flame 144 (2006) 1–16.
53. H.N. Najm, P.H. Paul, C.J. Mueller, P.S. Wyckoff, Combust. Flame 113 (1998) 312–332.
54. A. W. Skiba , T. M. Wabel , J. E. Temme , J. F. Driscoll, Measurements to Determine the Regimes of Turbulent Premixed Flames, AIAA Paper 2015-4089.
55. A. Marshall, P. Venkateswaran, D. Noble, J. Seitzman, T. Lieuwen, *Expt. Fluids* 51 (2011) 611–620.
56. B. Videto, D. Santavicca, *Combust. Sci. Technol*. 76 (1991) 159–164.
57. J. O. Hinze , Turbulence, McGraw Hill Pub, New York NY, 1959.
58. Mayo, W.T. Jr., A discussion of limitations and extensions of power spectrum estimation with burst-counter LDV systems. International workshop on laser velocimetry, West Lafayette, Indiana, Purdue University, pp 90-101, 1974.
59. Tummers, M.J., Passchier, D.M. Spectral estimation using a variable window and the slotting technique with local normalization. Meas. Sci. Technol. 7:1541-1546, 1996.
60. Wu, H., Patterson, G.K, Chemical Engineering Science, Vol. 44, No. 10, p. 2207, 1989.

APPENDIX A. Details of the PLIF and LDV Diagnostics

Simultaneous formaldehyde-OH PLIF signals were acquired at 2.5 Hz by two Andor iStar intensified CCD cameras. Each 1024 by 1024 pixel image was binned (2 x 2) to create a spatially-averaged image consisting of 512 x 512 pixels. Formaldehyde was excited by the third harmonic of a Spectra-Physics Nd:YAG laser operating at 355 nm and approximately 135 mJ/pulse. The fluorescence was filtered using high and low pass filters (CG385 and BG3, respectively) that transmitted wavelengths between 385 and 490 nm. The OH beam was excited using a second Spectra-Physics Nd:YAG laser that pumped a Sirah dye laser. The dye laser output was at 566.45 nm, which was then doubled using a BBO crystal to 283.22 nm to excite the Q1(7) transition of OH [21]. Typical laser power was 4.5 mJ/pulse at 283.22 nm. The OH camera was equipped with a band pass filter centered at 310 +/- 5 nm. Gate times for both cameras were limited to 100 ns and the laser pulses were separated by 250 ns to avoid cross talk [22]. The laser sheet thicknesses were measured by traversing a razor blade across the beam waist; the 283 nm beam was 180 μm thick while the 355 nm beam was 325 μm thick, between locations where laser intensity was $1/e^2$ of the maximum . The simultaneous PLIF setup is shown in Figure 14.

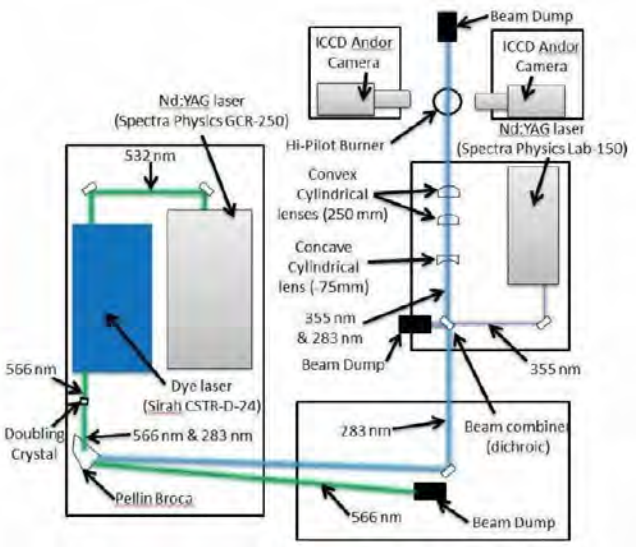

Figure 19. Simultaneous OH-formaldehyde PLIF diagnostics

Image post-processing involved the following steps. First, for each PLIF image the corrected signal (S) was determined at each pixel from:

$$S = [(R-D) - (B-D) - (F-D)] / C \qquad (17)$$

R is the uncorrected raw signal, D is the dark noise, B is the background radiation with no flame, F is the flame radiation with the laser off and C is the sheet correction factor. The raw image (R) is the image recorded by the camera after a spatial filter was applied. The value of each pixel is set to the median value of a 2 pixel by 2 pixel region. The dark noise image is the average of 200 (?) images when all light is blocked from entering the lens. D is typically 2% of the maximum raw signal. The background image B is measured when the flame is turned off but the laser sheet is on. The flame radiation is measured with the flame on and with the laser sheet turned off. The sheet correction factor (C) is determined by recording the light from a white field created by uniformly illuminating a white sheet of paper.

The pixels in the OH camera had to be registered (aligned in space) with the pixels in the formaldehyde camera. A target was placed at the location of the laser sheet; the target is a thin transparent sheet with crosses printed on both sides. From the target images recorded by the two cameras, two transform matrices were computed that relate each pixel in each camera the its proper (x, y) location in the laser sheet. Then the product of each pair of OH and formaldehyde images was computed on a pixel by pixel basis. If the resulting product for a pixel was below a threshold value, the pixel value was set to zero.

A Laser Doppler Velocimeter (LDV) provides measurements of the velocity fluctuations and the integral scales at an axial location 5 mm downstream of the burner exit and at various radial locations. An Argon-Ion laser operating at 1.5 Watts (Coherent Innova 90c) and a commercial Doppler burst correlator (TSI FSA 4000) recorded the axial component of velocity. The tracer species used in this experiment was 0.5 μm alumina-oxide particles, while the optical components and photomultiplier tube consisted of standard commercial LDV equipment (TSI, Inc.)

1.

1. Report Type

Final Report

Primary Contact E-mail
Contact email if there is a problem with the report.

jamesfd@umich.edu

Primary Contact Phone Number
Contact phone number if there is a problem with the report

734-936-0101

Organization / Institution name

University of Michigan

Grant/Contract Title
The full title of the funded effort.

Premixed Turbulent Combustion in High Reynolds Number Regimes

Grant/Contract Number
AFOSR assigned control number. It must begin with "FA9550" or "F49620" or "FA2386".

FA9550-12-1-0101

Principal Investigator Name
The full name of the principal investigator on the grant or contract.

James F. Driscoll

Program Manager
The AFOSR Program Manager currently assigned to the award

Dr. Chiping Li

Reporting Period Start Date

03/15/2012

Reporting Period End Date

03/14/2016

Abstract

The physics of turbulent premixed flames, in the range of the high Reynolds numbers that are associated with Air Force applications, was measured for the first time using advanced laser imaging diagnostics. Combustion in three regimes on the Borghi regime diagram of premixed turbulent flames was quantified for the first time, by imaging the thicknesses of preheat and reaction layers. New PLIF diagnostics were developed, due to our interactions with Dr. Cam Carter at AFRL to image reactions zones with a new CH PLIF method, as well as using the overlap method that involves formaldehyde and OH PLIF. Results are used to assess previous theoretical predictions of regime boundaries. PLIF images of CH, OH and formaldehyde were
obtained for thirteen cases. The three regimes are (a) the thickened preheat (TP) regime that is bounded by the Klimov-Williams limit, (b) the broken reaction layers (BR) boundary that is bounded by Norbert Peters predicted limit, and the partially-distributed reactions (PDR) regime.
A new Hi-Plot burner provides "extremely-turbulent" flames (defined to be values of u'/SL between 24 and 243) which is up to ten times that of previous experiments. It was found that the measured thickened preheat (TP) boundary is in approximate agreement with the Klimov-Williams prediction, but that the broken flamelet (BF) boundary measurements

do not agree with the Peters prediction. Partially distributed reactions (PDR) are local blobs of distributed reactions that are connected by thin flamelets. They were found to be associated with either merging or breaking of the flamelets. Globally-distributed reactions were not observed. There was no evidence that distributed reaction occur due solely to layer broadening, as has been predicted. Preheat layer thickness was ten times the laminar value but reaction layers were not broadened. Residence time of eddies in the flame (which scales as x/U) is important since the flame tip has reactions that are broader, broken and more distributed than at the flame base.

Distribution Statement

This is block 12 on the SF298 form.

Distribution A - Approved for Public Release

Explanation for Distribution Statement

If this is not approved for public release, please provide a short explanation. E.g., contains proprietary information.

SF298 Form

Please attach your SF298 form. A blank SF298 can be found here. Please do not password protect or secure the PDF The maximum file size for an SF298 is 50MB.

AFD-070820-035.pdf

Upload the Report Document. File must be a PDF. Please do not password protect or secure the PDF . The maximum file size for the Report Document is 50MB.

AFD-070820-035.pdf
3 Final rept.pdf

Upload a Report Document, if any. The maximum file size for the Report Document is 50MB.

Archival Publications (published) during reporting period:

A. W. Skiba, T. M. Wabel, J. E. Temme, and J. F. Driscoll, Measurements to Determine the Regimes of Turbulent Premixed Flames 51st AIAA/SAE/ASEE Joint Propulsion Conference, AIAA Paper 2015-4089, submitted for journal publication.

A. W. Skiba, T. M. Wabel, J. E. Temme, and J. F. Driscoll, Experimental Assessment of Premixed Flames Subjected to Extreme Turbulence 54th AIAA Aerospace Sciences Meeting, AIAA Paper 2016-1454, submitted for journal publication.

Changes in research objectives (if any):

none

Change in AFOSR Program Manager, if any:

none

Extensions granted or milestones slipped, if any:

one year no-cost extension granted

AFOSR LRIR Number

LRIR Title

Reporting Period

Laboratory Task Manager

Program Officer

Research Objectives

Technical Summary

Funding Summary by Cost Category (by FY, $K)

	Starting FY	FY+1	FY+2
Salary			
Equipment/Facilities			
Supplies			
Total			

Report Document

Report Document - Text Analysis

Report Document - Text Analysis

Appendix Documents

2. Thank You

E-mail user

Mar 10, 2016 12:26:26 Success: Email Sent to: jamesfd@umich.edu